

## Progress Towards a Gas-Flow Standard using Microwave and Acoustic Resonances

Accepted for publication in in Flow Measurement and Instrumentation, July 18<sup>th</sup>, 2019.

<https://doi.org/10.1016/j.flowmeasinst.2019.101592>

Jodie G. Pope<sup>a</sup>, Keith A. Gillis<sup>a</sup>, Michael R. Moldover<sup>a</sup>, James B. Mehl<sup>b</sup>, and Eric Harman<sup>c</sup>.

<sup>a</sup> *Fluid Metrology Group, NIST, Gaithersburg, MD 20899, USA*

<sup>b</sup> *36 Zunuqua Trail, P.O. Box 307, Orcas, WA 98280-0307, USA*

<sup>c</sup> *Colorado Engineering Experiment Station, Inc (CEESI), USA*

### Abstract

We describe our progress in developing a novel gas flow standard that utilizes 1) microwave resonances to measure the volume, and 2) acoustic resonances to measure the average gas density of a collection tank / pressure vessel. The collection tank is a 1.85 m<sup>3</sup>, nearly-spherical, steel vessel used at pressures up to 7 MPa. Previously, using the cavity's microwave resonance frequencies, we determined the cavity's pressure- and temperature-dependent volume  $V_{\text{BBB}}$  with the expanded uncertainty of 0.022 % (coverage factor  $k = 2$ , corresponding to 95 % confidence level). This was the first step in developing a pressure, volume, speed of sound, and time (*PVwt*) primary standard. In the present work, when the shell was filled with argon, measurements of pressure and acoustic resonance frequencies determined the "acoustic mass"  $M_{\text{acst}}$  that agreed with gravimetric measurements within 0.04 %, even when temperature gradients were present. Most of these differences were a linear function of pressure; therefore, they can be reduced by further research. We designed and implemented a novel positive feedback system to measure the acoustic resonance frequencies. Using the measurements of  $V_{\text{BBB}}$ , pressure, and acoustic resonance frequencies of the enclosed gas (nitrogen or argon), we calibrated 3 critical flow venturis that NIST has used as working standards for over 10 years. The two independent flow calibrations agreed within the long-term reproducibility of each CFV, which is less than 0.053 %. Furthermore, the feasibility of a dynamic tracking technique using this feedback loop was tested by comparing  $\Delta M_{\text{acst}}$  computed under no-flow conditions and  $\Delta M_{\text{acst}}$  computed by the rate of fall or rise during a flow. This was done for flows ranging from 0.11 g/s to 3.9 g/s.

Keywords: flow standard; collection volume; calibrated volume; gas source; acoustic resonator; microwave resonator.

## Nomenclature

$a$	Inner radius of the BBB from microwave measurements	$M_{\text{BBB}}$	Mass of gas in the BBB
$A$	Throat area of a CFV	$M_{\text{acst}}$	Mass determined from $f_{0n}^{\text{a,c}}$
BBB	“Big Blue Ball”; spherical shell	$M_{\text{grav}}$	Mass determined by weighing
$c_0$	Speed of light in vacuum	$M_w$	Molar mass
$C^*$	Critical flow factor that accounts for real-gas properties in flows through a CFV	$P$	Pressure <sup>1</sup>
CFV	Critical flow venturi	$R$	Universal gas constant
$C_d$	Discharge coefficient for a CFV	$\rho$	Mass density
$f$	Subscript “f”; final conditions	$S$	Sensitivity coefficient = $\partial x / \partial y \cdot y / x$
$f_{\text{br}}$	Breathing mode frequency of the BBB shell.	$T$	Kelvin temperature <sup>1</sup>
$f_{0n}^{\text{a}}$	Measured resonance frequency of the $n^{\text{th}}$ radial acoustic mode of a gas in a quasi-spherical cavity.	$t$	time
$f_{0n}^{\text{a,c}}$	Resonance frequency of the $n^{\text{th}}$ radial acoustic mode of a gas in a quasi-spherical cavity, corrected for perturbations due to shell motion, imperfect shape, and heat exchange at the gas-shell interface	$U_e$	Expanded uncertainty ( $k = 2$ , 95 % confidence level)
$f_{\ell n}^{\text{m},\sigma}$	Resonance frequency of the $\sigma \ell n$ microwave mode of a gas-filled spherical cavity with conducting walls; $\sigma = \text{TM}$ (transverse magnetic) or $\text{TE}$ (transverse electric)	$u$	Standard uncertainty ( $k = 1$ , 68 % confidence level)
$\varphi$	Acoustic velocity potential	$V_{\text{BBB}}$	Internal volume of the BBB from microwave measurements including addenda.
$\gamma_0$	$= C_p^0 / C_v^0$ : Specific heat ratio of a gas at zero pressure	$V_{\text{gas}}$	Internal volume of the BBB including addenda determined by gas expansion
$i$	Subscript “i”; initial conditions	$w$	Speed of sound at $T$ and $P$
$\dot{m}$	Calibrated mass flow	$Z$	$= M_w P / (\rho RT)$ ; Compressibility factor
$\dot{m}_{\text{th}}$	Theoretical (uncalibrated) mass flow from a CFV	$Z_a$	$= M_w w^2 / (\gamma_0 RT)$ ; squared ratio of speed of sound to its zero-pressure value
		$\xi_{0n}^{\text{a}}$	Eigenvalue of $n^{\text{th}}$ radial acoustic mode of a gas in a perfectly spherical cavity
		$\xi_{\ell n}^{\text{m},\sigma}$	Eigenvalue of the $\sigma \ell n$ microwave mode in a spherical cavity with conducting walls; $\sigma = \text{TM}$ (transverse magnetic) or $\text{TE}$ (transverse electric)

<sup>1</sup> Unless otherwise denoted,  $T$  and  $P$  refer to the gas in the BBB.

## 1. Introduction

During 2016, the value of natural gas metered in pipelines in the United States was approximately \$90 billion. To ensure equity at each transfer of custody, accurate metering is required, both in the US and international markets. NIST calibrates natural gas flow meters and has an ongoing research program to improve the accuracy of these calibrations [1]. At present, NIST traces the calibration of pipeline-scale natural gas flowmeters to NIST's primary gas flow standard that uses the pressure, volume, temperature, and time (*PVTt*) technique [2] and air as the calibration gas. This primary standard relies on a well-characterized, carefully-thermostated [ $U(T) = 12 \text{ mK}$ ]<sup>2</sup>, 0.67 m<sup>3</sup> collection vessel that operates at pressures up to 0.15 MPa. The primary standard is used to calibrate, one at a time, 21 critical flow venturis (CFVs), each with throat diameter of 5.2 mm. The 21 CFVs are used in parallel to calibrate several 25 mm-diameter CFVs, one at a time [3]. This use of 21 CFVs in parallel is the first of 6 stages of scale-up that uses both CFVs and turbine meters. The scale-up begins with air flows of  $\approx 10 \text{ g/s}$  and ends with flows of natural gas encountered in large natural gas pipelines:  $\approx 500 \text{ kg/s}$  at pressures near 7 MPa. Each stage of scale-up adds cost and uncertainty to the calibration of large meters. The purpose of this work is to reduce the number of stages in the traceability chain by starting with a novel, primary gas-flow standard that makes large, low uncertainty gas flow standards practical. The new standard uses acoustic resonance frequencies to determine the average speed of sound. The speed of sound is combined with the pressure to determine the average density of the gas (either argon or nitrogen) in the standard. This circumvents the need to measure the average temperature of the gas. At present, conversion from air calibrations to natural gas calibrations occurs at flows of 14 kg/s, which is beyond the range of this work. Therefore, we will not conduct natural gas calibrations with the novel primary standard described here.

In a prior publication [4], we characterized a 1.85 m<sup>3</sup> nearly spherical pressure vessel informally called the big blue ball (or BBB) to be used as the gas collector or gas source for flow calibrations. (See Fig. 1.) By measuring the frequencies of a few microwave resonances in the BBB's internal cavity, we determined the BBB's internal volume  $V_{\text{BBB}}$  with the uncertainty of 0.022 % ( $k = 2$ ) while the  $V_{\text{BBB}}$  was filled with either nitrogen or argon at pressures ranging from 30 kPa to 7 MPa

---

<sup>2</sup> Unless otherwise stated, all uncertainties are expanded uncertainties that use the coverage factor  $k = 2$  corresponding to 95 % confidence level.

and at temperatures ranging of 293 K to 298 K. We also studied the approach to equilibrium of  $P/(f_{0n}^a)^2$ , where  $f_{0n}^a$  is the resonance frequency of the  $n^{\text{th}}$  radial acoustic mode of the gas, immediately after pumping gas into or bleeding gas out of the BBB to see how soon  $M_{\text{acst}}$  could be determined when thermal gradients generated by flow work were present. Because temperature measurements of the internal gas are not necessary for the new flow standard, the mass could be determined before the BBB returned to an isothermal state. The fast relaxation of  $M_{\text{acst}}$  is a distinct advantage of the acoustic method of determining  $M_{\text{BBB}}$ . Instrumentation and transducers used to measure the acoustic resonance and microwave frequencies are described in our prior publication [4].



**Figure 1.** The 1.85 m<sup>3</sup> BBB is welded to and supported by a cylindrical pedestal. Two flanged ports are visible. The BBB's wall is 19 mm (3/4 inch) thick; the pedestal is made from 6.3 mm (1/4 inch) thick plate.

In this work, we filled the BBB with aliquots of argon gas and measured the pressure and the frequencies  $f_{0n}^a$  of three radially-symmetric acoustic resonances of the argon. These frequencies were corrected for the recoil vibrations of the shell, the thermal boundary layer where the argon contacts the shell's inner surface, and the ports welded to the shell. The corrected frequencies  $f_{0n}^{\text{a,c}}$  were used to determine the speed of sound  $w$  in the argon. The mass of argon ( $M_{\text{acst}}$ ) in the BBB was deduced from the measured pressure and speed of sound using thermodynamic data from the literature [5]. Remarkably, to first order in the magnitude of the temperature variation, this method to determine  $M_{\text{acst}}$  does not require knowledge of the temperature distribution of the gas within the BBB. Figure 4a shows a comparison between  $M_{\text{acst}}$  and  $M_{\text{grav}}$ , the mass of gas in the BBB determined by a weighing (gravimetric) technique. The fractional differences  $(M_{\text{acst}} - M_{\text{grav}})/M_{\text{grav}}$  range from  $-0.03\%$  to  $+0.04\%$ .

Finally, as a proof of principle, we used the BBB as a source of high-pressure argon or nitrogen to measure the flow through three critical flow venturis (CFVs) that have a 10-year-long calibration history based on NIST's 677 L primary  $PVT_t$  standard [2]. The BBB-based measurements were conducted using a standing start-stop method where the pressure and  $f_{0n}^{a,c}$  were measured before the flow was started and after the flow had been stopped. The discharge coefficients  $C_d$  were consistent within the long-term reproducibility of each CFV, which is less than 0.053%. Furthermore, the feasibility of a dynamic tracking technique using this feedback loop was tested by comparing  $\Delta M_{acst}$  computed under no-flow conditions and  $\Delta M_{acst}$  computed by the rate of fall or rise during a flow. This was done for flows ranging from 0.11 g/s to 3.9 g/s. Further tests under more extreme flow conditions are needed to validate the dynamic tracking technique.

Considered as a gas-collection vessel, the BBB has a maximum operating pressure that is 55× larger than NIST's 677 L  $PVT_t$  standard [2]. The past work [4] was an interim step towards gas-flow measurements traced to standards of frequency and pressure, and to the literature of  $\rho(P,w)$  data. This contrasts with NIST's existing gas-flow measurements that are traced to standards of temperature and pressure and to literature data for the compressibility factor  $Z(P,T)$  [5]. If this work is successful, it will reduce the cost and uncertainty of the scale-up chain, thereby improving equity in large-scale natural gas transactions.

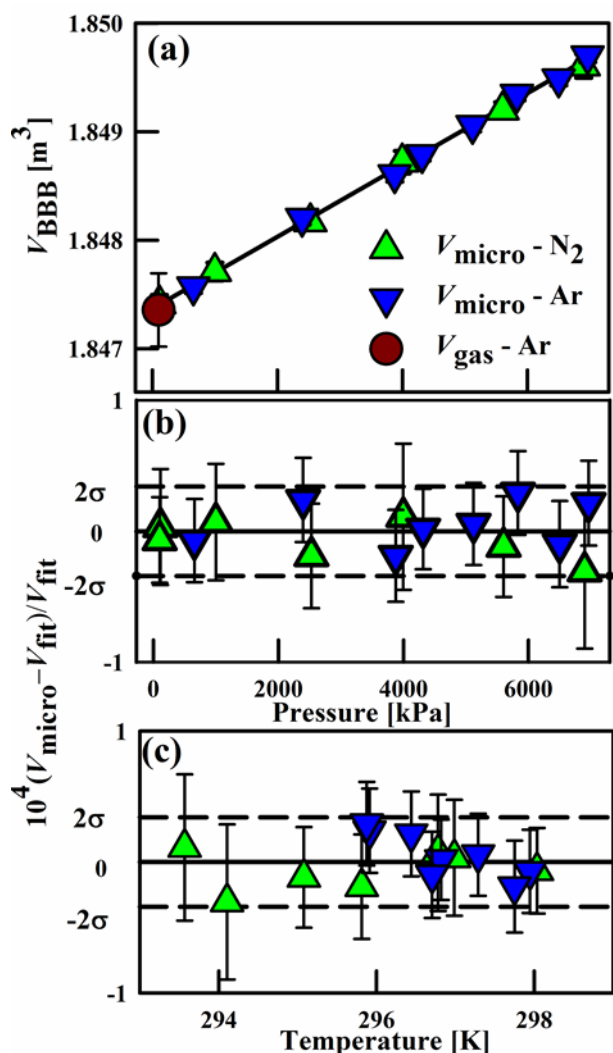


**Figure 2.** (a) Pressure-dependent volume of the BBB at 295 K measured using microwaves and gas expansion. (b) fractional volume deviations from Eq. (2) as a function of pressure at 295 K, and (c) as a function of temperature at 0 MPa. The errors bars are one standard deviation of the measurements made with 3 microwave modes. The fractional standard deviation of the data from the fit was  $\sigma = 17 \times 10^{-6}$ , which corresponds to a random uncertainty of 0.32 K in the average temperature of the BBB.

## 2. Summary of Volume Measurements

In a previous conference publication [4], we used the relation

$$f_{ln}^{m,\sigma} = \frac{\xi_{ln}^{m,\sigma} c_0}{2\pi n_g a} \quad (1)$$

to determine the internal spherical volume  $V_{\text{BBB}}$  from the measured resonance frequencies  $f_{ln}^{m,\sigma}$  of three microwave modes (TM13, TE12, and TE13) while the BBB was filled with nitrogen or argon at pressures ranging from 0 MPa to 7 MPa. (Here,  $n_g$  is the refractive index of the gas,  $c_0$  is the defined value of the speed of light,  $\xi_{ln}^{m,\sigma}$  is a microwave eigenvalue, and  $a$  is the average radius of the BBB.) The volume and its uncertainty ( $k = 2$ ) are summarized by

$$\begin{aligned} V_{\text{BBB}}(P, T_{\text{sh}}) &= 1.84740 [1 + 3\alpha_T(T_{\text{sh}} - 295 \text{ K}) + \kappa P] \text{ m}^3 (\pm 0.022\%), \\ \alpha_T &= 1.75 \times 10^{-5} \text{ K}^{-1} (\pm 8.1\%), \\ \kappa &= 1.790 \times 10^{-4} \text{ MPa}^{-1} (\pm 1.3\%) \end{aligned} \quad (2)$$

We measured the shell temperature  $T_{\text{sh}}$  in Eq. (2) with four thermistors attached to the outer surface of the BBB. Figure 2 displays  $V_{\text{BBB}}(P, T_{\text{sh}})$  and the deviations from Eqs. (2). In [4], we also used a gas expansion technique to independently measure the volume  $V_{\text{gas}}$  of the BBB at 0.1 MPa and 295 K. At this  $P$  and  $T$ , the expanded uncertainty of the microwave-based volume measurements was 0.007 % while the expanded uncertainty of the gas expansion approach was 0.018 %. The volumes of the BBB measured by the two techniques agreed within 0.002 %, well within the root-sum-of-squares (RSS) of the two approaches at 0.1 MPa and 295 K (0.019 %,  $k = 2$ ) (Fig. 2a).

Our previous publication describes the microwave antennas, the microwave frequency measurements, and the volumes of the addenda (sealed ports and drain tube) that were included in the gas-expansion volume but not in the microwave-determined volume. The volumes of the addenda were determined from dimensional measurements and are included in  $V_{\text{BBB}}$ . The refractive indices of nitrogen and argon were required to deduce  $V_{\text{BBB}}$  from the measured microwave frequencies. These refractive indices were estimated from values of the dielectric constants taken from the NIST Standard Reference Database 23, Version 9.1, known as ‘‘REFPROP’’ [5]; their uncertainties were a negligible contributor to the uncertainty of  $V_{\text{BBB}}$ . If water vapor is present in such test gases, its high polarizability must be included when computing the refractive index at microwave frequencies.

### 3. Determinations of mass by gravimetric ( $M_{\text{grav}}$ ) and acoustic ( $M_{\text{acst}}$ ) techniques.

This section describes two independent determinations of the mass of argon contained within the BBB. We demonstrate the degree of consistency between these mass determinations and discuss their uncertainties. For the conventional mass determination, we weighed aliquots of argon gas in the range  $6 \text{ kg} \leq \Delta M_{\text{grav}} \leq 28 \text{ kg}$  before adding them into the BBB. For the novel acoustic mass determination, we used Eqs. (2) through (4) together with measurements of the pressure  $P$  and resonance frequencies  $f_{0n}^a$  of 3 radially-symmetric acoustic modes ( $n = 3, 4, 5$ ) of the argon in the BBB. (See [6] for the mode notation and for details concerning the measurement and correction of acoustic resonance frequencies.) After each aliquot of argon was added to the BBB, we monitored  $f_{0n}^a$  for one acoustic mode and waited sufficient time for  $P/(f_{0n}^a)^2$  to stabilize before determining  $M_{\text{acst}}$ . At 4.3 MPa and 294 K these frequencies were nominally 577 Hz, 815 Hz, and 1052 Hz and their quality factors [7] were approximately 25000, 58000, and 34000, respectively. The measured acoustic frequencies were corrected for the motion of the BBB's shell, the ports, and for heat exchange in the boundary layer where the argon contacts the shell. The corrected frequencies (superscript "c") and their respective eigenvalues  $\xi_{0n}^a$  were combined with the average radius  $a$  of the BBB deduced from  $V_{\text{BBB}}$  to determine an average speed of sound  $w$  in the argon using

$$w = \frac{2\pi a f_{0n}^{\text{a,c}}}{\xi_{0n}^a}. \quad (3)$$

We combined  $P$ ,  $f_{0n}^{\text{a,c}}$ ,  $V_{\text{BBB}}$ , and literature values of  $w$  using Eqs. (2) and (3) to compute  $M_{\text{acst}} \equiv \rho(P, w)V_{\text{BBB}}$

$$M_{\text{acst}} = \frac{\gamma_0 P V_{\text{BBB}}}{w^2} \frac{\mathcal{Z}_a}{Z} = \frac{\gamma_0 P a}{3\pi} \left( \frac{\xi_{0n}^a}{f_{0n}^{\text{a,c}}} \right)^2 \frac{\mathcal{Z}_a}{Z}. \quad (4)$$

In Eq. (4),  $Z \equiv M_w P / (\rho R T)$  is the compressibility factor of argon,  $M_w$  is the molar mass,  $\rho$  is the mass density, and  $\mathcal{Z}_a = M_w w^2 / (\gamma_0 R T)$  is the squared ratio of the speed of sound to the speed of sound at zero pressure at the same temperature. We used REFPROP [5] to compute  $w^2$ ,  $\mathcal{Z}_a$ , and  $Z$  at pressures ranging from vacuum to 7 MPa and temperatures ranging from 285 K to 305 K in

5 K increments. We fit a rational polynomial to the quantity  $z_a/Z$  as a function of  $P$  and  $w^2$ , thereby eliminating the need for temperature measurements.

### 3.1 Weighing Argon Aliquots

To weigh aliquots of argon, we assembled the apparatus shown in Fig. 3. This apparatus consisted of an aluminum frame and two 48 L, commercially-manufactured, high-pressure aluminum cylinders (DOT specification 3AL-2216). The apparatus had a flexible hose that was always attached to the aluminum cylinders but could be connected and disconnected from the BBB with negligible gas loss. Both cylinders were filled with argon to 12.4 MPa. The apparatus was then weighed on a calibrated



**Figure 3.** Weighing apparatus used to validate mass measurements using acoustic resonance frequencies.

scale that had a resolution of 1 g. After weighing, the flexible hose was connected to the BBB and the argon in both cylinders was discharged until the pressure equilibrated. Then the flexible hose was disconnected from the BBB and the apparatus was weighed again. The difference between initial and final buoyancy-corrected weights yielded the mass of one aliquot of argon. As indicated in Table 1, 16 aliquots were added to the BBB. Because the initial pressure in the weighing apparatus was always 12.4 MPa and because pressure was increasing in the BBB, each succeeding aliquot was 5 % smaller, on average, than the preceding one. The first aliquot was 19.6 kg while the 16<sup>th</sup> aliquot was 5.7 kg. As the argon was delivered from the weighing apparatus to the BBB, the apparatus cooled and water condensed on the tanks. We used a fan to aid in evaporation during and after the fills until the tanks appeared dry and the mass on the weigh scale was stable for more than 5 minutes.

The largest contribution to the uncertainty of the mass of each aliquot was  $u(\Delta M_{\text{grav}}) = \sqrt{2}(1 \text{ g})/\Delta M_{\text{grav}}$ , where “1 g” is resolution of the weigh scale and the factor  $\sqrt{2}$

**Table 1. Comparison of the argon aliquot masses determined by weighing  $M_{\text{grav}}$  and determined from the average of the (0,3), (0,4) and (0,5) acoustic modes  $M_{\text{acst}}$ .**

aliquot	$P$ [MPa]	Cumulative $M_{\text{grav}}$ [kg]	$\langle M_{\text{acst}} \rangle$ [kg]	$U_e(M_{\text{acst}})$ [%]	$U_e(M_{\text{grav}})$ [%]	$\frac{100 \times (\langle M_{\text{acst}} \rangle - \sum \Delta M_{\text{grav}})}{\sum \Delta M_{\text{grav}}}$ [%]
1	0.65619	19.646	19.642	0.072	0.018	-0.021
2	1.26082	38.102	38.097	0.066	0.020	-0.014
3	1.84526	55.944	55.936	0.064	0.021	-0.015
4	2.39477	72.957	72.948	0.064	0.022	-0.013
5	2.91422	89.086	89.080	0.064	0.022	-0.007
6 <sup>a</sup>	3.41975	104.064	104.073 <sup>a</sup>	0.064	0.022	-0.013 <sup>a</sup>
7&8	4.31586	132.393	132.400	0.064	0.023	0.005
9&10	5.12034	157.618	157.640	0.065	0.023	0.014
11&12	5.83931	181.183	181.218	0.065	0.023	0.019
13&14	6.50154	201.781	201.829	0.066	0.023	0.024
15&16	6.96411	216.970	217.019	0.066	0.023	0.023

<sup>a</sup>At 3.4 MPa, the values of  $M_{\text{acst}}$  from the (0,3) and (0,5) modes were outliers; therefore, they were omitted from the analysis.

accounts for the two independent weighings that are required to determine each value of  $\Delta M_{\text{grav}}$ . Smaller uncertainty contributions come from the buoyancy corrections and the pressure expansion of the cylinders in the weighing apparatus. The results of the gravimetric mass determinations and their uncertainties are listed in Table 1, together with the corresponding results from the acoustic mass determinations. Figure 4a shows agreement between the two methods well within their combined uncertainties indicated by the dashed lines. Table 1 gives the uncertainties for both  $M_{\text{grav}}$  and  $M_{\text{acst}}$ .

### 3.2 Cumulative Measurements of $M_{\text{acst}}$

If other sources of uncertainty (*e.g.* transients when the flow starts and stops and measurements of  $P$  and  $T$  at the meter under test) are small,  $U_e(M_{\text{acst}})$  is relevant to a flow calibration that starts with an evacuated BBB and collects a mass of argon equal to  $\sum \Delta M_{\text{grav}}$ . Below, we also used the same data to estimate the uncertainties of acoustic mass *differences*  $\Delta M_{\text{acst}}$  generated by one or two aliquots. These difference estimates are relevant to a flow calibration that starts with a partially filled BBB and collects or dispenses a mass of argon equal to a single aliquot. Finally, we discuss contributions to  $U_e(M_{\text{acst}})$  resulting from uncertain speed-of-sound data  $w(P,T)$ , pressure transducers, impurities in the gas, and incomplete thermal equilibration during the acoustic measurements.

Figure 4a displays the differences (in percent) between the acoustic mass  $M_{\text{acst}}$  and the cumulative mass of the argon aliquots  $\sum_0^P \Delta M_{\text{grav}}$  as a function of pressure. (At the maximum pressure, 7 MPa, the BBB contained approximately 217 kg of argon.) At each pressure,  $M_{\text{acst}}$  was deduced independently from the (0,3), (0,4), and (0,5) modes using Eqs. (2) – (4). All the values of  $M_{\text{acst}}$  fall within  $-0.03\%$  to  $+0.04\%$  of  $M_{\text{grav}}$ . The data used to generate Fig. 4a are listed in Table 1. In Fig. 4, small mutual inconsistencies are visible between the values of  $M_{\text{acst}}$  determined by the three modes. This is emphasized by the equally-weighted straight-line fits to the values of  $M_{\text{acst}}$  plotted for each mode. The inconsistencies span  $\pm 0.004\%$  at 0.66 MPa and  $\pm 0.018\%$  at 7 MPa.

The origin of these inconsistencies is unknown; therefore, we choose to treat them as a pressure-dependent uncertainty. A linear fit was applied to the standard deviation of the mean in the three measured acoustic modes at each pressure, the resulting expression for this uncertainty is:

$u = 0.0032\% + 9.18 \times 10^{-7}(P)\%$ , where  $P$  is in kPa. This component contributes more to  $U_e(M_{\text{acst}})$  as the mass in the BBB increases. However, as discussed in Section 3.5, the pressure measurement is the largest contributor to the combined uncertainty in  $M_{\text{acst}}$  ( $> 80\%$  at all pressures), and therefore, this pressure dependent contribution contributes, at most,  $8.5\%$  to  $U_e(M_{\text{acst}})$ .

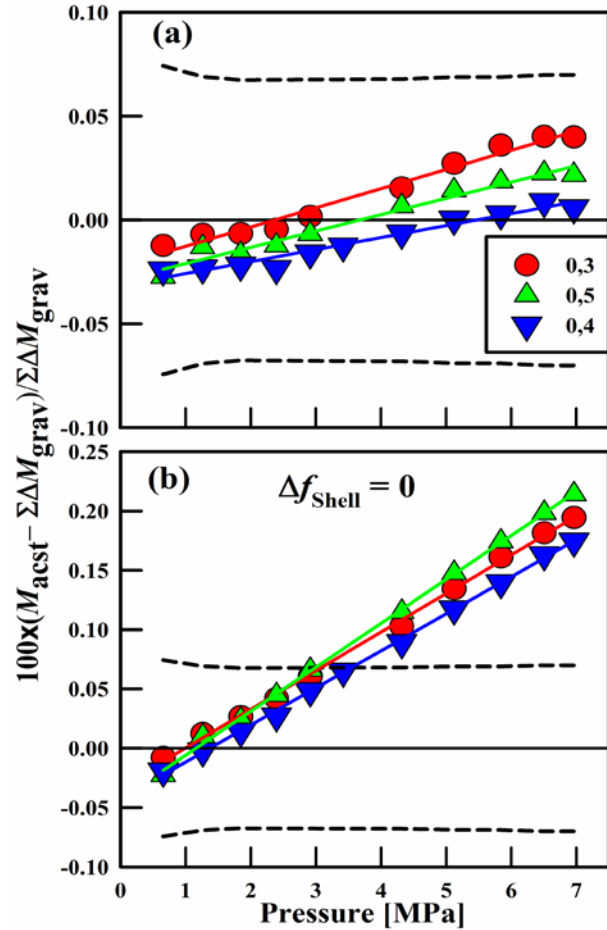


**Figure 4.** Comparison of cumulative mass of argon aliquots, as determined by weighing ( $M_{\text{grav}}$ ) and by the (0,3), (0,4), and (0,5) acoustic modes ( $M_{\text{acst}}$ ). For both panels, the dashed curves are the  $k = 2$  RSS uncertainties in  $M_{\text{grav}}$  and  $M_{\text{acst}}$ . The solid lines represent unweighted fits to the values of  $M_{\text{acst}}(P)$  for each mode. The shell correction  $\Delta f_{\text{sh}}$  was applied to the acoustic data in panel 4a, but not in panel 4b.

### 3.3 The Correction $\Delta f_{\text{shell}}$ for Momentum Exchange Between the Shell and the Gas

The terms in Eqs. (3) and (4) that are most-likely to account for the inconsistent values of  $M_{\text{acst}}$  for the 3 modes are the corrections to the measured acoustic frequencies. Because the inconsistencies have a near-linear pressure dependence, we suspect that they originate in the imperfections of the correction  $\Delta f_{\text{shell}}$ . This correction accounts for momentum exchange between the BBB's spherical shell and the radially-symmetric gas resonances. We calculated  $\Delta f_{\text{shell}}$  using the expression

$$\frac{\Delta f_{\text{shell}}}{f} = -\frac{\rho w^2}{a} \left( \frac{\partial a}{\partial P} \right)_s \frac{1}{1 - (f/f_{\text{br}})^2} \quad (5)$$

which is adapted from Eq. (86) from [8]. Here,  $f_{\text{br}} \approx 1854$  Hz is the frequency of the radially-symmetric (“breathing”) oscillations of an ideal, thin spherical shell which we estimated<sup>3</sup> using Eqs. (43) and (86) of [8]. In Eq. (5),  $(\partial a/\partial P)_s$  is the adiabatic compliance of the shell's radius to internal pressure. We note that the term  $\rho w^2 \approx \gamma_0 P$  is approximately proportional to the pressure. The proportionality constant  $\gamma_0$  is the ideal-gas heat-capacity ratio  $C_P^0/C_V^0$ , which is 5/3 for argon and approximately 1.4 for nitrogen. Thus,  $\Delta f_{\text{shell}}/f$  is approximately proportional to the pressure with a frequency-dependent proportionality constant that varies as  $[1 - (f/f_{\text{br}})^2]^{-1}$ .

To determine the speed of sound  $w$  in the gas,  $\Delta f_{\text{shell}}$  must be subtracted from the measured acoustic resonance frequencies. A comparison of Figs. 4a and 4b indicates that the correction  $\Delta f_{\text{shell}}$  contributes, at most,  $0.002 M_{\text{acst}}$  to the value of the acoustic mass  $M_{\text{acst}}$ . To achieve an uncertainty  $u(M_{\text{acst}}) = 0.025\%$  ( $k = 1$ ), the shell correction must have an uncertainty  $u(\Delta f_{\text{shell}}) \leq u(M_{\text{acst}})/(0.002) = 13\%$ . This tight tolerance led us to consider the difference between the adiabatic and isothermal deformations of the shell. (This difference was not considered in Refs. [6] and [8] because these earlier works only considered acoustic resonances in thick shells and low pressures where  $\Delta f_{\text{shell}}/f_{0n}$  was much smaller than in this work.) To estimate  $f_{\text{br}}$  and  $(\partial a/\partial P)_s$  in Eq. (5), we used the thermodynamic relation  $k_T = k_S + [(\partial V/\partial T)_P/V]^2 T/(\rho C_P)$  between the isothermal and adiabatic compressibility,  $k_T$  and  $k_S$ , respectively. We evaluated  $k_T$  using literature values for Poisson's ratio (0.297), the isobaric specific heat ( $C_P \approx 500$  J kg<sup>-1</sup> K<sup>-1</sup>), and the density (7960 kg/m<sup>3</sup>) of carbon steel. We also used our microwave-determined values of the isothermal

---

<sup>3</sup>Eq. (43) of Ref. [8] should be corrected to read:  $c_{\text{sh}} = [(\lambda + 2\mu)/\rho_{\text{sh}}]^{1/2}$

compliance of the shell  $(\partial a/\partial P)_T$  and the linear coefficient of thermal expansion  $\alpha_T$  given in Eq. (2). This estimate yields  $(\partial a/\partial P)_S \approx 0.96 \times (\partial a/\partial P)_T$ . We were not able to estimate the uncertainty of the factor 0.96 because we do not know the alloy from which the BBB was manufactured.

The model for  $\Delta f_{\text{shell}}$  leading to Eq. (5) assumes that the shell's elastic response is radially symmetric when the shell's motion is driven by any radially-symmetric acoustic mode. The BBB's departures from spherical symmetry included: 1) a supporting pedestal welded to bottom of the BBB, 2) ports containing transducers and antennas welded to the shell, and 3) the joint between the two hemispheres consisting of a circumferential, full-penetration groove weld with a backing ring in the BBB. These asymmetries led us to measure the radial acceleration of the BBB's surface with accelerometers bonded to the exterior of the shell while the BBB contained nitrogen at 7 MPa; the nitrogen was driven by the acoustic source at the resonance frequency of either the (0,3), (0,4), or (0,5) mode. We found that the shell did not oscillate in a radially-symmetric pattern. It was obvious that the pedestal supporting the BBB constrained the motion of the lower half of the BBB. (Approximately, the BBB weighed 1100 kg and the pedestal weighed 100 kg.) For each of the nitrogen resonances, the oscillation of the BBB's volume was approximately consistent with Eq. (5). A more precise statement would require acoustic transducers that were calibrated at high pressures; such transducers were not available to us. When the BBB was evacuated, and the shell was driven by a shaker, many resonances were observed; these resonances were not modelled. Our observations do not quantitatively explain the mode-dependence of  $M_{\text{acst}}$ ; however, such a mode dependence is not surprising.

In the future, we will not weld a shell such as the BBB to its supports. We note isothermal compliance of the shell  $(\partial a/\partial P)_T$  is inversely proportional to the shell's thickness. Therefore,  $\Delta f_{\text{shell}}$  (and its mode-dependence) might be reduced either by using a thicker shell (relative to its radius) and/or by restricting the use of the BBB to pressures well below 7 MPa.

### 3.4 Incremental Measurements of $\Delta M_{\text{acst}}$

The points plotted in Fig. 5 represent the fractional differences between  $\Delta M_{\text{grav}}$  and  $\Delta M_{\text{acst}}$ , the difference between the acoustically determined mass of the gas in the BBB before and after adding the aliquot as calculated by Eq. (6).

$$\Delta M_{\text{acst}} = \frac{\gamma_0 (\xi_{0n}^a)^2}{3\pi} \left[ \frac{P_f a_f}{(f_{0n,f}^{a,c})^2} \left( \frac{Z_a}{Z} \right)_f - \frac{P_i a_i}{(f_{0n,i}^{a,c})^2} \left( \frac{Z_a}{Z} \right)_i \right] \quad (6)$$

Above 4 MPa, two aliquots were used to generate  $\Delta M_{\text{grav}}$  and  $\Delta M_{\text{acst}}$ . The dashed curves represent the ( $k = 2$ ) RSS uncertainties of  $\Delta M_{\text{grav}}$  and  $\Delta M_{\text{acst}}$ . The scatter of the incremental values of  $\Delta M_{\text{acst}}$  in Fig. 5 is substantially larger than the scatter of the cumulative values of  $M_{\text{acst}}$  in Fig. 4 for two reasons: 1) for the cumulative values, the BBB was evacuated before the 16 aliquots were admitted into the BBB; therefore, the starting value of  $M_{\text{acst}}$  was essentially zero with zero uncertainty, and 2) except for the first aliquot, the cumulative mass and the pressure changes during the cumulative measurements were several times larger than the corresponding changes for the incremental measurements. The incremental determinations of  $\Delta M_{\text{acst}}$  required measuring a small pressure difference in the presence of a large total pressure. Therefore,  $U_e(\Delta M_{\text{acst}})$  is larger than  $U_e(M_{\text{acst}})$ .

The uncertainty curves in Fig. 5 demonstrate how the uncertainty in  $\Delta M_{\text{acst}}$  increases as  $\Delta P$  decreases with each successive mass aliquot. The relative partial derivative of Eq. (6) with

**Table 2. Example uncertainty budget for  $\Delta M_{\text{acst}}$  for a 0.9 MPa pressure increase (28 kg argon mass increase) and initial  $P_{\text{BBB}}$  of 4.3 MPa. (This table uses the “bad” sensor in Section 3.5.1 because we used it for the mass validation experiments).**

Component	$u$ [%]	% Contribution
BBB radius	$3.3 \times 10^{-3}$	0.85
BBB pressure	0.033	84.6
Acoustic frequency	$3.6 \times 10^{-3}$	0.98
Real gas correction	$7.8 \times 10^{-3}$	4.7
$P$ -dependent mode inconsistency	0.011	8.69
$U_e(k=2)$ [%]	<b>0.082</b>	

respect to all of the variables is inversely proportional to  $\Delta M_{\text{acst}}$ . Therefore,  $\Delta M_{\text{acst}}$  must be large enough to obtain the desired

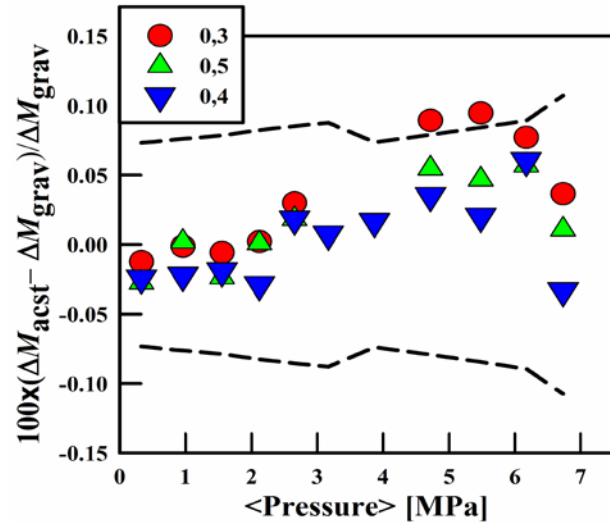


**Figure 5. Comparison of the mass of each argon aliquot, as determined by weighing ( $M_{\text{grav}}$ ) before admitting the aliquot into the BBB and as determined from the difference in  $M_{\text{acst}}$  before and after admitting the aliquot into the BBB. The dashed curves are the  $k = 2$  RSS uncertainties in  $M_{\text{grav}}$  and  $M_{\text{acst}}$ . The horizontal coordinate of each plotted point is the average of the pressures measured before and after adding the aliquots.**

uncertainty when performing flow calibrations. Table 2 gives an example of the uncertainty budget for a 0.9 kPa pressure change in the BBB, the largest pressure change during these experiments.

### 3.5 Other Contributions to the Uncertainty of $\Delta M_{\text{acst}}$

In the zeroth-order approximation,  $M_{\text{acst}} = (\gamma_0 P V_{\text{BBB}}/w^2)(1 + \dots)$ . Here, we consider contributions to  $U_c(\Delta M_{\text{acst}})$  from pressure measurements, uncertain speed-of-sound data, and impurities in the argon that change  $\gamma_0$ . In our previous publication [4] and in Section 4.2 below, we describe a possible systematic error in  $M_{\text{acst}}$  due to nonlinear temperature gradients in the BBB. This systematic error depends on the orientation of the gradient, the geometry of the vessel, and the acoustic modes used. Our calculations predict that the longitudinal acoustic modes in a horizontal cylindrical with vertical gradients give the correct average to determine  $M_{\text{acst}}$ .

#### 3.5.1 Pressure Transducers.

The average of two, nominally-identical, pressure transducers were used for the mass determinations with argon gas. These transducers have a history of stable calibrations dating back to 2001, less than 0.06 % change between calibrations, but significant zero drifts, as much as 0.15 Pa/day, required daily correction. The sensors were calibrated from 0.1 MPa to 7 MPa at the beginning of the mass determination experiments and at the completion. One of the transducers had a calibration shift as large as 0.051 %, the second had a calibration shift as large as 0.035 % over the range of calibration. The standard deviations of the calibration data from a 3<sup>rd</sup> order polynomial function of the pressure were 0.006 % for one sensor and 0.004 % for the other sensor. The two sensors always had a discrepancy of 150 Pa to 200 Pa at all pressures where measurements were made. The sensors were re-zeroed when the discrepancy got larger than 200 Pa.

Because we are measuring pressure differences and the differences are measured within a 24 h period, the uncertainty associated with the sensors' calibration is treated as completely correlated. However, the degree of correlation of the discrepancy between the sensors is not known. Because we do not know the degree of correlation, the discrepancy is treated as non-correlated. The relative standard uncertainty in the initial pressure ( $P_i$ ) and final pressure ( $P_f$ ) measurements from the calibration is  $u(\text{cal}) = 0.031\%$ . The discrepancy between the two sensors is treated as a uniform

(or rectangular) distribution with a relative uncertainty of  $u(\text{disc}) = (200 \text{ Pa} / P_{\text{meas}}) / \sqrt{3}$  for  $P_i$  and  $P_f$  measurements. The  $k = 2$  uncertainty is therefore,

$$U_e(\Delta P) = \frac{2}{(P_f - P_i)} \left\{ P_i^2 \left[ u(\text{cal})^2 + u(\text{disc})_i^2 \right] + P_f^2 \left[ u(\text{cal})^2 + u(\text{disc})_f^2 \right] - 2P_i P_f u(\text{cal}) \right\}^{1/2}. \quad (7)$$

The smallest  $\Delta P = P_f - P_i$  during the mass validation experiments was 462.6 kPa (Table 1, final aliquot into BBB). For this pressure change,  $U_e(\Delta P) = 0.09\%$ . The pressure measurements are the largest contributors to the overall uncertainty in  $\Delta M_{\text{acst}}$  regardless of the pressure change. For flow measurements we obtained two sensors with improved calibration stability, zero drift stability and the discrepancy between the two sensors was less than 100 Pa. For  $\Delta P = 462.6$  kPa, the new sensors decrease  $U_e(\Delta P)$  to 0.04 %.

### 3.5.2 Speed-of-Sound Data.

The experiments discussed in this work were conducted using “ultra-high purity” grade argon and dry nitrogen from a liquid dewar. The argon supplier stated that the impurity concentrations were less than 0.001 %. We used a chilled mirror hygrometer to verify that the dew point of argon pumped out of the BBB was less than  $-40$  °C (the lower limit of the dew point sensor) after the argon had resided inside the BBB for many days at 6.9 MPa.

For the thermophysical properties of argon, we used the correlation of Tegeler *et. al.*, [9] as implemented in REFPROP [5]. For argon, REFPROP provides the correct ideal-gas speed of sound and specifies: “The estimated uncertainty of calculated speeds-of-sound is in general less than 0.02 %.” This specification includes the possibility that the REFPROP’s values of  $w^2$  are in error by 0.04 % at 7 MPa; such an error might account for the average slope of the lines in Fig. 4; therefore, we were motivated to review the measurements of  $w^2$  reported by Estrada-Alexanders and Trusler [10]. Throughout the range of our measurements, the speed-of-sound data of Estrada-Alexanders and Trusler have the remarkably small fractional uncertainty  $u(w) \leq 10^{-5}$ . Along the isotherms at 300 K and 350 K, the fractional differences between their measurements and REFPROP are at most  $(w_{\text{data}} - w_{\text{REFPROP}}) / w_{\text{REFPROP}} \leq 1.4 \times 10^{-5}$ . In a first approximation,  $M_{\text{acst}} \propto P/w^2$ ; therefore, the argon data or the REFPROP representation of the argon data will contribute

only a few parts in  $10^5$  to  $u(M_{\text{acst}})$ . We also considered the acoustically determined mass increment  $\Delta M_{\text{acst}}$  between the beginning and the end of a flow calibration:  $\Delta M_{\text{acst}} \propto [(P/w^2)_f - (P/w^2)_i]$ . We calculated these differences using REFPROP and using the data of Estrada-Alexanders and Trusler for the pressure increments used in their measurements (1.3 MPa to 2.1 MPa). The largest difference was less than 0.01 % of  $\Delta M_{\text{acst}}$ . We conclude that uncertainty contributions to  $\Delta M_{\text{acst}}$  resulting from the uncertainty of the speed-of-sound data in argon and their correlation in REFPROP are much smaller than other uncertainties.

For the thermophysical properties of nitrogen, we used the correlation of Span et. al., [11] as implemented in REFPROP. REFPROP uses the thermodynamic relation  $w^2 = (\partial P / \partial \rho)_s$  to generate values of the speed of sound. These values are consistent (within 0.003 % at 300 K for  $P \leq 7$  MPa) with the zero-frequency speed of sound deduced from measurements by Costa Gomes and Trusler [12] and the additional measurements reported by Estela-Uribe and Trusler [13]. Here, we briefly discuss why the zero-frequency speed of sound slightly underestimates the speed of sound determined from the acoustic resonance frequencies  $f_{0n}^a$  in the BBB. For nitrogen gas, the relaxation time  $\tau_{\text{vib}}$  for the equilibration between the vibrational and translational degrees of freedom is long:  $\tau_{\text{vib}} P > 0.1$  s·MPa at 295 K. During the present measurements, the maximum pressure was 6.5 MPa and the minimum frequency was  $f_{03}^a \approx 520$  Hz; therefore,  $\tau_{\text{vib}} \geq (0.1 \text{ s}\cdot\text{MPa}/6.5 \text{ MPa}) \gg 1/f_{03}$ . Thus, the vibrations of the nitrogen molecule did not have time to follow the acoustic temperature during each acoustic cycle. As discussed in [12], at 300 K the measured values of  $f_{0n}^a$  will exceed those calculated from the thermodynamic (zero-frequency) speed of sound by 0.0091 %. We corrected the REFPROP values of  $w^2$  for this effect; if we did not make the correction, we would have underestimated  $\Delta M_{\text{acst}}$  by 0.018 %.

#### 4. Flow Measurements

To demonstrate the principle of using the BBB to calibrate flowmeters and to learn what improvements are needed, we compare our novel *PVwt* standard to NIST's well-documented 677 L *PVTt* standard [2] using relatively small CFVs that have a 10-year calibration history. In this work, we performed standing start-stop flow measurements. Also, we tested the feasibility of using a dynamic method. The dynamic method is superior to the static method because it will

enable faster calibrations with lower uncertainty. In contrast with standing start-stop calibrations, dynamic calibrations do not have uncertainty contributions from flow transients at the start and stop nor do they have uncertainties from changes in the mass stored in connecting volumes. Our preliminary tests indicate that the dynamic measurements of  $M_{acst}$  are accurate even though thermal gradients are not stable.

Dynamic flow calibrations need fast-responding ( $< 5$  Hz) sensors to measure the pressure, frequency, and shell temperature of the BBB (for  $V_{BBB}$  calculations). We have learned that in future work we will need to better optimize our tracking abilities by using digital filters that can be incorporated into the data acquisition system. Furthermore, we will use a muffler to reduce interference from flow-generated noise.

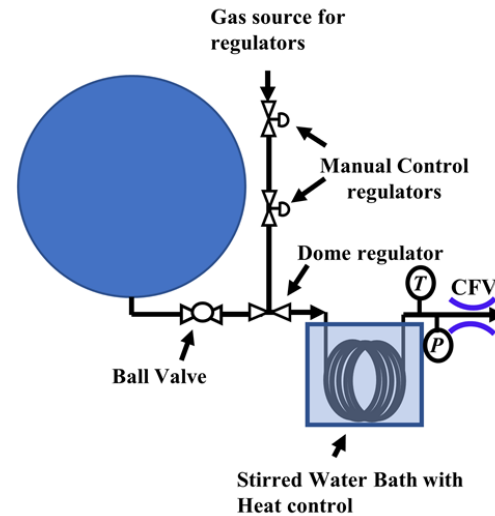


Figure 6. BBB initial flow test setup.

#### 4.1 Standing start-stop flow measurements with CFVs

The BBB was used as the gas source for the initial flow measurements using either ultra-high purity (UHP) argon or nitrogen gas from a liquid dewar. As shown in Fig. 6, the BBB was fitted with a ball valve at the outlet that started and stopped the flow. A non-venting dome regulator located downstream of the ball valve kept the pressure constant at the CFV. The dome regulator was controlled by two venting manual regulators. The gas exiting the dome regulator passed

Table 3. Results from initial standing start-stop flow tests performed using the BBB as a gas source.

CFV	$N$	$P_{CFV}$ [kPa]	$\dot{m}$ [g/s]	$\langle \Delta P_{BBB} \rangle$ [kPa]	$U_e(\Delta M_{acst})$ [%]	St. Dev. of Mean $C_d$ [%]	$U(\text{tails})^*$ [%]	$U_e(C_d)$ [%]
6.4 mm	1	619.4	45.43	1801	0.022	NA	0.018	0.068
6.4 mm	3	675.7	49.41	1813	0.024	0.008	0.032	0.075
6.4 mm	1	799.8	58.85	1646	0.033	NA	0.024	0.073
3.2 mm	4	482.6	11.23	500	0.051	0.041	0.064	0.13
3.2 mm	3	1041.1	19.02	1631	0.026	0.006	0.022	0.071
1.6 mm	3	965.3	5.69	370	0.047	0.011	0.016	0.081

\*The “tails” are the transients due to the start and stop of flow.

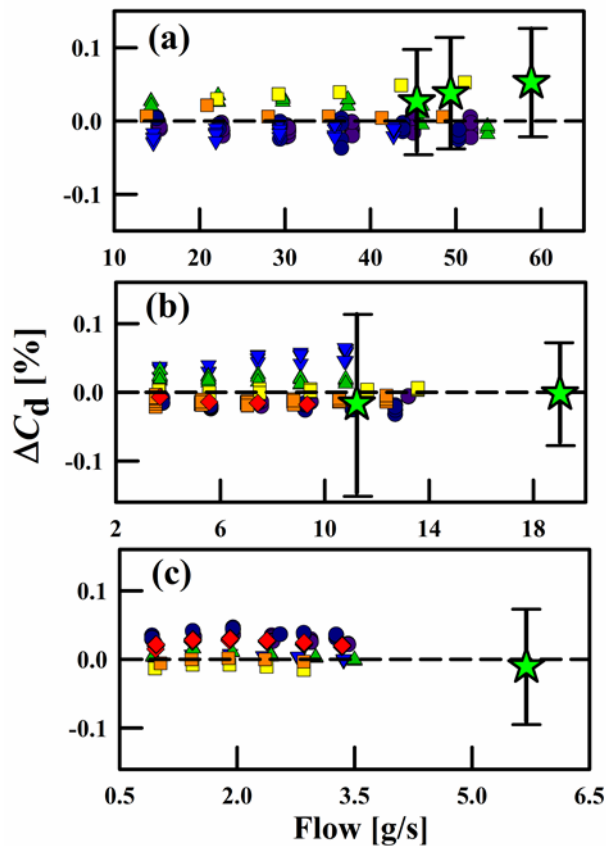


Figure 7. Comparison of discharge coefficients  $C_d$  of three CFVs measured with the BBB-standard (stars ★) with the historical (2008 to 2018) values of  $C_d$  measured with NIST's *PVTt* gas flow standard. The baselines are a weighted fit to the *PVTt* values of  $C_d$ . The uncertainty bars are  $k=2$  expanded uncertainties in  $C_d$ . The CFV throat diameters were (a) 6.4 mm, (b) 3.2 mm, and (c) 1.6 mm.

flow *PVTt* standard [2]. Table 3 gives the results of these measurements. Figure 7 compares the results to the 10-year calibration history for each CFV to the measurements made using the *PVwt* method.

The calibration factor of a CFV is called the discharge coefficient  $C_d$  calculated as

$$C_d = \frac{\Delta M_{\text{acst}}}{M_{\text{th}}}, \quad (8)$$

where the mass change in the BBB,  $\Delta M_{\text{acst}}$ , is determined from Eq. (6) and  $M_{\text{th}}$  is the uncalibrated, totalized mass that flowed through the CFV.

through a heat exchanger (coiled tube that was immersed in a thermostated, stirred water bath) before flowing through the CFV and into the ambient air. Because the gas was vented into the room, the volume between the BBB and the CFV was at atmospheric pressure before the flow interval started and after it stopped; therefore, the gas stored in this connecting volume was negligible. With the standing start-stop method, the uncertainty due to the initial and final flow transients (the “tails”) can be a significant portion of the overall flow uncertainty if the stable flow is not long enough. In the initial flow tests, these transients were significant.

The flow through three CFVs with nominal throat diameters of 6.4 mm (0.25 in), 3.2 mm (0.125 in), and 1.6 mm (0.063 in) was measured. The measurements were compared to calibrations performed on NIST's primary gas

To determine  $M_{acst}$ , we developed a novel method to measure the instantaneous resonance frequency  $f_{0n}^a$ . As indicated in Fig. 8, we used a positive feedback loop to excite self-oscillation of the desired acoustic mode. Self-oscillation was initiated by either ambient acoustic noise or an impulse to the BBB's shell (for example, by striking it with a rubber mallet). The signal from the microphone was amplified, filtered, phase shifted, and then fed back to the speaker in the BBB. For the amplitude to build, the loop gain must be greater than unity, and the feedback signal must

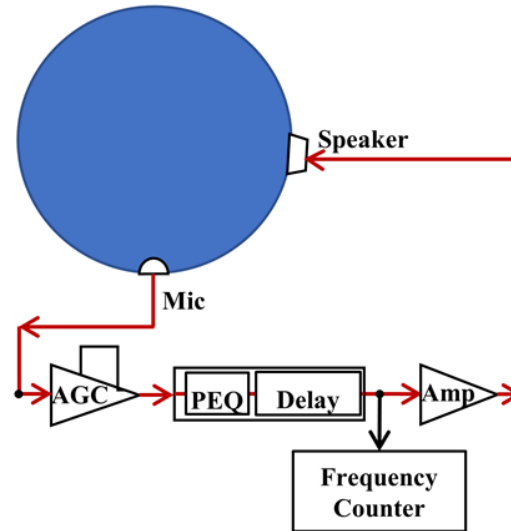


**Figure 8.** Positive feedback loop creates self-oscillation to track the frequency of a desired resonance. The feedback loop consists of an automatic gain control (AGC), a parametric equalizer (PEQ), a digital delay, and an output amplifier. The frequency is measured with a counter.

generate acoustic pressure that is in-phase with the acoustic field in the BBB. To ensure that only the desired acoustic mode was excited, we used a digital parametric equalizer (Behringer, DEQ 2496)<sup>4</sup> to reject frequencies outside of a narrow band approximately centered on the targeted resonance frequency. We used the digital delay module (integral to the DEQ 2496) to adjust the phase of the feedback signal to compensate for phase shifts introduced by the transducers and the electronics. If the phase of the feedback signal is improperly adjusted, then the oscillation frequency will differ slightly (by up to a halfwidth) from the natural frequency. When the loop is open, the oscillation can only occur at the natural frequency as the amplitude decays. Thus, we can measure the resonance frequency as the signal amplitude “rings down”. We did this for the (0,3), (0,4), and (0,5) modes. The pressure and frequency are measured simultaneously in real time for a few minutes and  $M_{acst}$  is determined from each acoustic mode before the start of and after the stop of the flow to obtain  $\Delta M_{acst}$ .

During the flow, we measured the stagnation temperature and pressure at the CFV and computed the theoretical mass flow through the CFV, defined as

<sup>4</sup> To describe materials and procedures adequately, it is occasionally necessary to identify commercial products by manufacturers' name or label. In no instance does such identification imply endorsement by the National Institute of Standards and Technology, nor does it imply that the particular product or equipment is necessarily the best available for the purpose.

$$\dot{m}_{\text{th}} = P_{\text{CFV}} A C^* \sqrt{\frac{M_w}{RT_{\text{CFV}}}} \quad (9)$$

where  $M_w$  is the molar mass of argon or nitrogen,  $R$  is the universal gas constant,  $T_{\text{CFV}}$  is the stagnation temperature at the CFV,  $P_{\text{CFV}}$  is the stagnation pressure at the CFV,  $A$  is the throat area of the CFV, and  $C^*$  is a thermodynamic property calculated via REFPROP. We computed the totalized mass through the CFV used in Eq. (8) from  $M_{\text{th}} = \sum_{i=1}^N \frac{1}{2} (\dot{m}_{\text{th},i} + \dot{m}_{\text{th},i+1}) (t_{i+1} - t_i)$ .

The uncertainty budget for the discharge coefficient is shown in Table 4 for the case of the 6.4 mm (0.25 in) and a mass flow of 45.4 g/s. In this case, the instability of the discharge coefficient, determined by years of calibration [14], is the largest contributor to the overall uncertainty. However, if the pressure change in the BBB is not sufficiently large,  $\Delta M_{\text{acst}}$  can become the largest contributor. In this case, it is the third largest contributor to the overall uncertainty. We assume that we know the pressure at the CFV within 50 Pa and the temperature within 100 mK from calibration data.

The initial flow tests show proof of concept by demonstrating agreement between NIST's existing gas flow standard and this novel *PVwt* standard. The largest gas flow NIST has performed with these CFVs using the 677 L *PVTt* standard is 52 g/s at pressure of 700 kPa. In this publication, we have pushed these limits slightly by going to 59 g/s and pressure of 800 kPa. The next generation acoustic standard will have a larger volume that will increase the achievable flows by an order of magnitude while maintaining a relatively "low" uncertainty. Therefore, we can use what we have learned here to aid us in the next design to make measurements more easily and to reduce the overall flow uncertainty. The calibrations made with the BBB used NIST's standards to measure the temperature and pressure at the CFV that are typically used during a gas flow calibration. These standards have high precision, but slow response time. Furthermore, the heat exchanger mentioned above was designed for relatively small flows and is not adequate for the magnitude of flows needed for our goal. A better designed heat exchanger and faster responding sensors will improve mass flow measurements at the CFV.

**Table 4: Uncertainty in  $C_d$  for 45.4 g/s flow through 6.4 mm CFV.**

Variable	$S$ [-]	$u$ [%]	$S^2 \times u^2$	% Contribution
$BBB \Delta M_{acst}$	1	0.012	$1.4 \times 10^{-4}$	10
$C_d$ stability*	1	0.025	$6.3 \times 10^{-4}$	44
$P_{CFV}$	1	0.0043	$1.8 \times 10^{-5}$	1.3
$T_{CFV}$	0.5	0.035	$3.0 \times 10^{-4}$	21
start/stop transients	1	0.016	$2.6 \times 10^{-4}$	18
Std Dev of Mean	1	0.008	$6.8 \times 10^{-5}$	4.9
		$u_c (k = 1)$	<b>0.038</b>	
		$U_c (k = 2)$	<b>0.075</b>	

\* This refers to the long-term stability in  $C_d$  from phenomena including mishandling of the CFV, reproducibility of the primary calibration standard, environmental conditions, thermal expansion and contraction of the CFV throat, thermal boundary layer formation in the throat during calibration, and sampling errors in the temperature at the CFV. See reference [14], page 18 for a full description.

#### 4.2 Dynamic flow measurements of $\dot{m}_{acst}$

Dynamic flow measurements are desirable because the measurement timings from the CFV and the BBB are synchronized. Therefore, flow transients caused by starting and stopping the flow can be completely neglected, and only the data from stable flow are used to compute the mass flow  $\dot{m}$  from the acoustic standard and the CFV.

Large, complex temperature gradients are generated by flow work as gas flows into or out of the BBB. When the flow is stopped, the complex temperature gradients quickly relax by convection leaving a vertically-stratified temperature field with warmer gas near the top of the cavity, cooler gas near the bottom. Our previous work [4] showed a systematic discrepancy in the acoustically measured mass until sufficient time had elapsed after the flow had stopped. In that work, we used a crude frequency tracking method with a lock-in amplifier and slow pressure sensors ( $< 0.25$  Hz). The lock-in amplifier was not able to keep track of a resonance frequency during a flow due to the fast-changing frequency. However, we were able to track a resonance frequency once the flow stopped. This prototype tracking technique led us to our previous conclusion that we had to wait for the temperature gradients in the BBB to become stable.

In this work, we designed and tested an improved tracking method that uses positive feedback to stimulate self-oscillation as discussed in Section 4.1. This improved method together with an improved data acquisition system enables nearly instantaneous measurements of the pressure and the resonance frequency, even while the pressure and the temperature gradients are changing

during flow. Over the range of flows tested so far (up to 4 g/s), the improved dynamic tracking method successfully tracked the resonance frequency. However, we have not yet tested dynamic tracking for the larger flows that are the goal of this resonance-base standard. Our future measurements will determine the flow limits and conditions for which the dynamic method is valid.

The expression for the mass in Eq. (4) assumes that the density is uniform throughout the volume. As discussed in [4] and [15], when gradients are present (say, due to flow work), the density must be averaged over the volume of gas  $\langle \rho \rangle_V \propto \langle 1/T \rangle_V$ . To first order in the magnitude of the temperature variation, the resonance frequency is determined by a weighted average of  $\langle w^2 \rangle_\phi \propto \langle T \rangle_\phi$  over the volume of gas. Here,  $\phi$  is the acoustic velocity potential [8], and the average is weighted by  $|\phi|^2$ . If the temperature gradients are sufficiently small, then  $\langle 1/T \rangle_V \approx 1/\langle T \rangle_V \approx 1/\langle T \rangle_\phi$ . For linear gradients,  $\langle T \rangle_\phi$  is identically equal to  $\langle T \rangle_V$ . For non-linear gradients, the differences between  $\langle 1/T \rangle_V$  and  $1/\langle T \rangle_\phi$  may be significant. From perturbation theory, the systematic error between  $\langle T \rangle_V$  and  $\langle T \rangle_\phi$  is dependent on the geometry of the vessel, the acoustic mode used, and the orientation and spatial dependence of the temperature gradient. We conclude from our calculations that the systematic error due to a vertical nonlinear temperature gradient will be much smaller if we use the longitudinal acoustic modes of a horizontal cylindrical vessel compared to the BBB [4].

When we perform quasi steady-state measurements of  $P$  and  $f_{0n}^a$  before the flow starts and after the flow stops to compute the mass of gas in the BBB using Eq. (4), we refer to these measurements as “static” because there is no flow. Such measurements are identical to the standing start-stop measurements mentioned in the previous section. Six tests were performed where  $\Delta M_{acst}$  was determined by static measurements and by tracking the (0,4) mode during a flow. Flows ranged from 0.11 g/s to 3.9 g/s. The feedback loop depicted in Fig. 8 was established and  $f_{04}^a$  and  $P$  were recorded simultaneously during a flow. Five tests were performed while releasing nitrogen gas from the BBB and one test was performed while filling the BBB with nitrogen. Because a flow regulator was used, the mass change in the BBB was a linear function of time. Figure 9 shows  $M_{acst}$  as a function of time while flowing nitrogen gas into the BBB at 3.9 g/s. The slope of the

mass versus time curve was calculated and multiplied by the elapsed time between the start and stop of the flow to obtain  $\Delta M_{acst}$ . In these preliminary tests, the elapsed time led to significant uncertainty in  $\Delta M_{acst}$ . Because our data acquisition system runs at about 0.2 Hz, we have, without corrections, approximately  $\pm 4.5$  s of uncertainty in the time of flow. We only need to know the absolute flow time to compare the dynamic and static measurements of  $\Delta M_{acst}$ . This equates to a  $k = 2$  uncertainty in the flow time ranging from 0.02 % (372-minute collection time) to 0.09 % (84-minute collection

time). In five out of these six tests, the  $k = 2$  error in the slope ranged from 0.002 % to 0.013 %; one test had some flow instabilities that increased this error to 0.22 %. Despite these extra hurdles to circumvent in the future,  $\Delta M_{acst}$  static agreed with  $\Delta M_{acst}$  dynamic within 0.13 %. Table 5 summarizes these results.

In this work the BBB was instrumented with two high-precision pressure transducers. The precision is a tradeoff for measurement acquisition speed (0.25 Hz). Furthermore, the frequency counter could only acquire data at 0.2 Hz limiting how quickly we could measure  $P/(f_{0n}^a)^2$ .

The dynamic tracking method is superior to the static measurement method because it has potential to enable faster flow calibrations with lower uncertainty. In future work we will better optimize our tracking abilities by using digital filters that can be incorporated into the data acquisition system. We will acquire faster responding pressure and temperature sensors that will enable tracking flows greater than we have demonstrated in this work. This is a great challenge because as the flow increases, greater temperature gradients in the BBB will be generated that change much more rapidly than what we have experienced here. Furthermore, the noise generated from the flow needs to be muffled to isolate the acoustic frequency of interest.

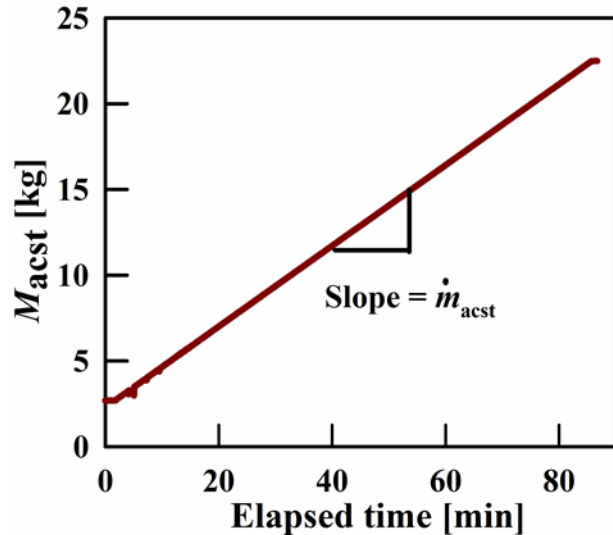


**Figure 9. Test of dynamic frequency tracking feedback loop. The mass of nitrogen gas flowing into the BBB from Eq. (4) while tracking the (0,4) mode as a function of time.**

**Table 5. Comparison of  $\Delta M_{\text{acst}}$  using the static method and the dynamic tracking method. The (0,4) acoustic mode was used for this comparison.**

$\langle \dot{m}_{\text{acst}} \rangle$	$\Delta P^{(a)}$	$\Delta t$	$10^2 \cdot \left( \frac{\Delta M_{\text{acst,dyn}}}{\Delta M_{\text{acst,stat}}} - 1 \right)$	$u(\Delta t)$	$u(\text{slope})$	$U_e(\Delta M_{\text{acst}})_{\text{stat}}$	$U_e(\Delta M_{\text{acst}})_{\text{dyn}}$
[g/s]	[kPa]	[min]	[%] <sup>(b)</sup>	[%]	[%]	[%]	[%]
0.11	-104	337	-0.13	0.020	0.007	0.20	0.20
0.15	-153	372	-0.05	0.009	0.002	0.14	0.14
0.54	-377	245	0.004	0.015	0.11 <sup>(c)</sup>	0.06	0.23
0.64	-174	95	-0.12	0.035	0.013	0.12	0.14
0.65	-317	172	-0.12	0.019	0.008	0.07	0.08
3.9	948	84	-0.07	0.043	0.010	0.03	0.09

<sup>(a)</sup> Negative values indicate gas release from the BBB.

<sup>(b)</sup> The subscripts “stat” and “dyn” denote the static and dynamic methods, respectively.

<sup>(c)</sup> This data set had “poor” flow control and hence a larger than typical error in the calculated slope.

## Conclusions

We have demonstrated that large resonators can be used as primary flow standards by achieving the following: 1) determining the volume of a quasi-spherical pressure vessel using microwave resonance frequencies, 2) validating the acoustic determinations of the mass of the gas in the BBB by comparisons with gravimetric measurements, and 3) validating BBB-based, standing start-stop calibrations of 3 CFVs by comparisons with their long-term calibration histories. In addition, we developed a novel feedback loop that enables measuring the integrated flow out of the BBB during intervals of a few minutes. This loop significantly reduced the time required to determine the resonance frequency without measuring the full resonance profile as described in [7]. We also demonstrated the ability of the novel feedback loop to track an acoustic frequency while gas flowed into or out of the BBB; thereby facilitating dynamic flow measurements.

In Section 3.3, we modeled the response of the BBB to the radial oscillations of the gas inside it by approximating the BBB as a thin, elastic, spherical shell. The elastic response made significant corrections to our mass determinations; however, the accuracy of the corrections was limited in hard-to-quantify ways because of the differences between the model and the BBB’s construction. These differences include: (1) The cylindrical pedestal welded to the BBB which had 9 % of the BBB’s mass, (2) the full groove weld and a backing ring that joined the two hemispheres comprising the BBB, and (3), four ports welded to the BBB. (We adapted the ports to accommodate instruments.) In the future, we will use a pressure vessel designed to have smaller, more-accurately-modelled, elastic corrections. The elastic corrections scale with the ratio (radius

of vessel)/(thickness of vessel's wall); therefore, to reduce the corrections, the next vessel will have thicker walls.

The next vessel will be a horizontal cylinder (with shallow, ellipsoidal headers) because the longitudinal acoustic modes in a horizontal cylinder are insensitive to linear, vertical temperature gradients [15]. In comparison with the radial modes of the BBB, we expect the longitudinal modes of the cylinder to give a more-accurate volume average of the gas's temperature, both during steady flows and as equilibrium is approached after a flow is stopped. The next vessel's ports will be installed at nodes of the acoustic pressure, where the ports will have the least effect on the acoustic resonance frequencies. To use the cylinder as a dynamic flow standard, we will incorporate digital filters in the feedback loop to track acoustic resonance frequencies during flow. Because flow noise increases with flow rate, successful tracking of high flows may require sophisticated averaging.

We plan to shorten the natural gas calibration chain by calibrating CFVs at pressures greater than 7 MPa. This will require a larger heat exchanger and improved flow control.

### **Acknowledgements**

The authors thank CEESI's management for their support and for lending the BBB to NIST. We thank Jim Filla for his continuing help with software development and Jim Schmidt for his help in developing the positive feedback method of frequency tracking.

### **References**

- 
- [1] A.N. Johnson, "Natural Gas Flow Calibration Service," NIST special publication 1081, August 2008. [www.nist.gov/publications/natural-gas-flow-calibration-service](http://www.nist.gov/publications/natural-gas-flow-calibration-service)
  - [2] J.D. Wright, A.N. Johnson, M.R. Moldover, and G.M. Kline, "Gas Flowmeter Calibrations with the 34 L and 677 L *PVTt* Standards," NIST Special Publication 250-63, November 2010. [www.nist.gov/publications/gas-flowmeter-calibrations-34-l-and-677-l-pvtt-standards](http://www.nist.gov/publications/gas-flowmeter-calibrations-34-l-and-677-l-pvtt-standards)
  - [3] A.N. Johnson, C. Li, J.D. Wright, G.M. Kline, and C.J. Crowley, "Improved Nozzle Manifold for Gas Flow Calibrations," 8<sup>th</sup> International Symposium on Fluid Flow Measurement, Colorado Springs, CO, U.S.; 6/18/2012 to 6/22/2012. [www.nist.gov/publications/improved-nozzle-manifold-gas-flow-calibrations](http://www.nist.gov/publications/improved-nozzle-manifold-gas-flow-calibrations)
  - [4] J.G. Pope, K.A. Gillis, M.R. Moldover, J.B. Mehl, and E. Harman, "Characterizing Gas-Collection Volumes with Acoustic and Microwave Resonances," 10<sup>th</sup> International Symposium on Fluid Flow Measurement, Queretaro, Mexico; 3/21/2018 to 3/23/2018.

---

www.nist.gov/publications/characterizing-gas-collection-volumes-acoustic-and-microwave-resonances

- [5] E.W. Lemmon, M.O. McLinden, and M.L. Huber, "REFPROP: Reference Fluid Thermodynamic and Transport Properties," NIST Standard Reference Database 23, Version 9.1, Natl. Inst. Stand. and Tech., Boulder, CO, (2010). [www.nist.gov/srd/nist23.cfm](http://www.nist.gov/srd/nist23.cfm)
- [6] M.R. Moldover, R.M. Gavioso, J.B. Mehl, L. Pitre, M. de Podesta, and J.T. Zhang, "Acoustic Gas Thermometry," *Metrologia* **51**, R1-R19 (2014).
- [7] M.R. Moldover, J.P.M. Trusler, and T.J. Edwards, "Measurement of the Universal Gas Constant R using a Spherical Acoustic Resonator," *Journal of Research of the National Bureau of Standards* 93-2, 85 – 144, (1988).
- [8] M.R. Moldover, J.B. Mehl, and M. Greenspan, "Gas-filled spherical resonators - Theory and experiment," *J. Acoust. Soc. of Am.* **79**, 253-272 (1986). Note: Eq. (43) of this reference should be corrected to read:  $c_{sh} = [(\lambda + 2\mu)/\rho_{sh}]^{1/2}$ .
- [9] Ch. Tegeler, R. Span, and W. Wagner, "A New Equation of State for Argon Covering the Fluid Region for Temperatures from the Melting Line to 700 K at Pressures up to 1000 MPa," *J. Phys. Chem. Ref. Data* **28**, 779-850 (1999).
- [10] A.F. Estrada-Alexanders, and J.P.M. Trusler, "The speed of sound in gaseous argon at temperatures between 110 K and 450 K and at pressures up to 19 MPa.," *J. Chem. Thermodynamics* **27**, 1075-1089 (1995).
- [11] R. Span, E.W. Lemmon, R.T. Jacobsen, W. Wagner, and A. Yokozeki, "A Reference Equation of State for the Thermodynamic Properties of Nitrogen for Temperatures from 63.151 to 1000 K and Pressures to 2200 MPa," *J. Phys. Chem. Ref. Data* **29**, 1361-1433 (2000).
- [12] M.C. Gomes, and J.P.M. Trusler, "The speed of sound in nitrogen at temperatures between  $T = 250$  K and  $T = 350$  K and at pressures up to 30 MPa," *J. Chem. Thermodynamics* **30**, 527-534 (1998).
- [13] J.F. Estela-Urbe and J.P.M. Trusler, "Acoustic and volumetric virial coefficients of nitrogen," *Int. J. Thermophysics* **21**, 1033-1044 (2000).
- [14] J.D. Wright, J.P. Kayl, A.N. Johnson, and G.M. Kline, "Gas Flowmeter Calibrations with the Working Gas Flow Standard," NIST Special Publication 250-80, November 2009. See page 18. <https://nvlpubs.nist.gov/nistpubs/Legacy/SP/nistspecialpublication250-80.pdf>
- [15] K.A. Gillis, J.B. Mehl, J.W. Schmidt, and M.R. Moldover, "Weighing' a gas with microwave and acoustic resonances," *Metrologia* **52**, 337-352 (2015).